Field-induced magnetic transitions in $Ca_{10}(Pt_3As_8)((Fe_{1-x}Pt_x)_2As_2)_5$ compounds

M. D. Watson,[1] A. McCollam,[2] S. F. Blake,[1] D. Vignolles,[3] L. Drigo,[3] I. I. Mazin,[4] D. Guterding,[5] H. O. Jeschke,[5] R. Valentí,[5] N. Ni,[6,7,8] R. Cava,[8] and A. I. Coldea[1,*]

[1]*Clarendon Laboratory, Department of Physics, University of Oxford, Parks Road, Oxford OX1 3PU, United Kindom*
[2]*High Field Magnet Laboratory, Institute for Molecules and Materials, Radboud University, 6525 ED Nijmegen, The Netherlands*
[3]*Laboratoire National des Champs Magnétiques Intenses (CNRS, INSA, UJF, UPS), Toulouse, France*
[4]*Code 6393, Naval Research Laboratory, Washington, DC 20375, USA*
[5]*Institut für Theoretische Physik, Goethe-Universität Frankfurt, 60438 Frankfurt am Main, Germany*
[6]*Department of Physics and Astronomy University of California, Los Angeles, USA*
[7]*Los Alamos National Laboratory, Los Alamos, New Mexico 87545, USA*
[8]*Department of Chemistry, Princeton University, Princeton, New Jersey 08544, USA*

(Received 15 October 2013; revised manuscript received 26 April 2014; published 30 May 2014)

We report a high magnetic field study up to 55 T of the parent and the nearly optimally doped iron-pnictide superconductor $Ca_{10}(Pt_3As_8)((Fe_{1-x}Pt_x)_2As_2)_5$ [$x = 0$ and 0.078(6)] using magnetic torque, tunnel diode oscillator technique, and transport measurements. We determine the superconducting phase diagram, revealing an anisotropy of the irreversibility field up to a factor of 10 near T_c and signatures of multiband superconductivity. Unexpectedly, we find a prominent anomaly in magnetic torque close to 22 T, when the magnetic field is applied perpendicular to the (ab) planes, which becomes significantly more pronounced as the temperature is lowered to 0.33 K. We suggest that this field-induced transition, observed both in the magnetically ordered parent compound and a nonordered superconducting sample, is a signature of a spin-flop-like transition associated not with long-range order but driven by antiferromagnetic fluctuations of magnetic moments aligned preferentially out of the conducting planes at low temperatures.

DOI: 10.1103/PhysRevB.89.205136 PACS number(s): 74.25.Bt, 74.20.Mn, 74.25.Dw, 74.70.Xa

I. INTRODUCTION

Superconductivity in Fe-based superconductors (FeBS) is believed to be mediated by magnetic fluctuations associated with the typical stripe order of the magnetic parent compound [1] that breaks the fourfold symmetry. Short-range antiferromagnetic fluctuations have been found to survive well above the Néel temperature and sometimes show *nematic* properties [2–6], that is, the simultaneous excitation of antiferromagnetic fluctuations with the same wave vector but different phases leading to orbital fluctuations and additional energy gain. In this paper, we present indirect evidence for the existence of antiferromagnetic fluctuations with preferential spin directions that manifest as a spin-flop-like transition in the torque measurements when the fluctuations slow down significantly at low temperatures and in high magnetic fields in a highly quasi-two-dimensional family of Fe-based superconductors.

Recently, $Ca_{10}(Pt_3As_8)(Fe_2As_2)_5$ (Ca-10-3-8) was found to be the parent compound of a new class of FeBS, the so-called 10-3-8 family [7]. The Fe-As layers are separated by Ca atoms and a Pt_3As_8 plane (Fig. 1) and the phase diagram is similar to other FeBS families. Recently, optical imaging [9], NMR [10], powder x-ray diffraction and μSR [11] have indicated structural and magnetic phase transitions in the parent 10-3-8 compound around 100 K, where the NMR measurement probing the ^{75}As environment suggests that the Fe-As planes have a striped antiferromagnetic order similar to $BaFe_2As_2$. Superconductivity occurs under applied pressure [12] or with electron doping, either by Ca for La [13], or Fe for Pt substitution [Fig. 1(a)]. The symmetries of the Fe-As and Pt-As planes are incompatible here, so the system crystallizes in the triclinic $P\bar{1}$ group [7]. However, because of the large separation of Fe-As and Pt-As layers the electronic properties of the Fe-As layer are expected to follow the tetragonal symmetry, as in other FeBS. This has been confirmed experimentally [14,15].

Here, we report high magnetic field studies up to 55 T of the nearly optimally doped $Ca_{10}(Pt_3As_8)((Fe_{0.922}Pt_{0.078})_2As_2)_5$, with $T_c \approx 10$ K and the parent compound. Using magnetic torque, tunnel diode oscillator (TDO) technique, and transport measurements, we determine the superconducting phase diagram, finding a high anisotropy up to $\gamma_H = 10$ near T_c and an irreversibility field up to 32 T. Furthermore, we find an anomaly at low temperatures at 22 T that is consistent with a spin-flop transition, when the magnetic field is applied perpendicular to the Fe-As planes and in close proximity to the superconducting phase. This anomaly is also observed in the undoped antiferromagnetic parent compound. The fact that this transition occurs both with and without any long-range magnetic order suggests that in the latter case it is due to antiferromagnetic fluctuations in the quasi-2D Fe planes. If the correlation length of these fluctuations is sufficiently large (several lattice parameters), the spins can opt to have their preferential spin orientation in the same way long-range ordered spins in the parent compound do.

The sample growth is described elsewhere [7]. Single crystal X-ray measurements confirmed the $P\bar{1}$ symmetry group. Wavelength-dispersive x-ray measurements in the doped sample give a doping level of $x = 0.078(6)$ by

*amalia.coldea@physics.ox.ac.uk

 ©2014 American Physical Society

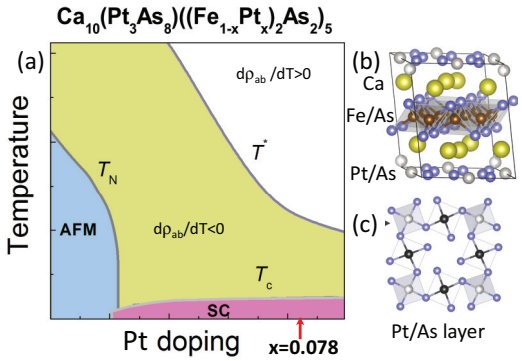

FIG. 1. (Color online) (a) Schematic phase diagram of $Ca_{10}(Pt_3As_8)((Fe_{1-x}Pt_x)_2As_2)_5$ as a function of electron doping x based on Refs. [7,8] with antiferromagnetic, superconducting, and semiconductinglike regions delimited by T_N, T_c, and T^*, respectively. The superconducting compound lies at the right of this phase diagram, as indicated by the arrow. (b) The structure of the 10-3-8 phase in which the Fe-As layers, Ca atoms and Pt-As layers [in (c)] form a layered structure that crystallizes in the low-symmetry $P\bar{1}$ triclinic space group.

constraining Fe + Pt = 13 in the chemical formula.[1] Transport measurements were performed in a Quantum Design PPMS in magnetic fields up to 14 T and also in pulsed fields up to 55 T at LNCMI, Toulouse with low-resistance electrical contacts made using Sn solder. Torque measurements were performed at low temperatures (down to 0.33 K) in magnetic fields up to 33 T at the HFML in Nijmegen and in pulsed fields up to 55 T at LNCMI in Toulouse. Single crystals with typical size $\approx 150 \times 150 \times 30\ \mu$m were used for torque measurements using highly sensitive piezo-resistive microcantilevers.

II. TORQUE MAGNETOMETRY

Figure 2 shows magnetic torque data on three crystals (superconducting S1, S2, and nonsuperconducting parent P1) when the field is approximately perpendicular to the ab planes. The typical hysteresis that occurs in the superconducting state due to the pinning of the flux vortices allows the determination of the superconducting phase diagram from the position of the irreversibility field H_{irr}, as indicated in Figs. 2(a) and 2(b). Furthermore, at magnetic fields above the superconducting hysteresis, we detect a clear anomaly at 22 T in the magnetic torque data that becomes sharper as the temperature is lowered to 0.33 K. This effect was reproduced in all the crystals investigated and no further anomalies were detected up to 55 T as shown in 2(f). This anomaly is well-defined only when the applied field is nearly perpendicular to the ab plane, and it is symmetric around this direction, as shown in Fig. 2(c). The width of this peak at H_M (the maximum in the torque signal after subtracting the featureless 9.6 K sweep), quantified by the half-width of Lorentzian fit to the subtracted data [inset of Fig. 2(b)], shows a linear decrease with decreasing temperature suggestive of slowing down of magnetic fluctuations and consequently the increase of their correlation length. The observed behavior of magnetic torque in 10-3-8 is rather unusual and in contrast to the $\tau \sim H^2 \sin(2\theta)$ background torque typically observed in other FeBS above and associated with paramagnetic behavior, as described in Appendixes A and B [16,17].

The transition in torque is accompanied by a change in slope in the longitudinal magnetization, $m_{\parallel}$, as shown in the inset of Fig. 2(f) and Appendix C. This can be easily understood by the fact that in the antiferromagnetic state there is no net magnetization, whereas in the spin-flop state there is an increasing magnetization along the direction of the field. The Zeeman energy makes this magnetization increasingly favorable, as shown in the inset of Fig. 2(f). Furthermore, we find that this anomaly is also present in the magnetically ordered parent compound ($x = 0$) [sample P1 in Fig. 2(e)]. The peak of the anomaly is slightly broader and shifted to higher fields in the parent compound, due to either a small misalignment between samples (close to $\boldsymbol{H} \perp ab$) or/and the degree of sample inhomogeneities. However, its evolution with temperature and its observation in a series of different samples, shown in Fig. 2, suggest that this anomaly is a clear characteristic of the $Ca_{10}(Pt_3As_8)((Fe_{1-x}Pt_x)_2As_2)_5$ compounds.

Next we discuss the possible scenarios to explain this field-induced magnetic anomaly. Firstly, we consider the role played by the 5d Pt ions that are heavy and have strong spin-orbit coupling, and may experience large magnetic anisotropy. In the doped material, there are two types of Pt: one in the Fe plane (Pt^{4+}) and another one in the Pt-As layer (Pt^{2+}).[2] We do not expect the latter to be magnetic, given the d^8 configuration of Pt^{2+}, but the former might spin polarize; even a weak polarization would provide a measurable anisotropy of the magnetic response. For this reason, we performed density functional theory (DFT) calculations on a $\sqrt{5} \times \sqrt{5}$ supercell with one Fe substituted by Pt (see Appendix A). We performed full lattice relaxation to avoid applying artificial internal pressure to the in-plane Pt. However, for both Pt positions (in-plane and intermediate layer) our calculations render completely polarization-free Pt, even though the surrounding Fe atoms acquire full polarization. Adding Hubbard $U = 2.5$ eV and $J = 0.5$ eV does not create spin polarization on Pt either.

Secondly, to understand our experimental findings, we look for spin-flop-like physics in the Fe subsystem. Although there is no reported long-range antiferromagnetic order in the superconducting compound ($x = 0.078$) (see Fig. 1), there are certainly antiferromagnetic fluctuations, which could become

[1]WDX was performed on several areas of a millimeter-sized crystal from the same batch as the samples in which the anomaly was observed. Our value of $x = 0.078(6)$ is found by constraining $N(\text{Fe} + \text{Pt}) = 13$. The point-to-point variation was on the order of the measurement uncertainty.

[2]The square-planar coordination of Pt in the Pt-As layer creates a strong crystal field, with a high antibonding $d_{x^2-y^2}$ band, and all other d states occupied, so the valency of the interlayer Pt is 2^+, as opposed to the Pt^{4+} substituting for Fe. The arsenics in the Pt_3As_8 plane form covalently bound dimers with an effective valency of 4^- per dimer so that the ionic electron count is $Ca_{10}^{2+}\ Pt_3^{2+}(As_2)_4^{4-}\ Fe_{10}^{2+}\ As_{10}^{3-}$.

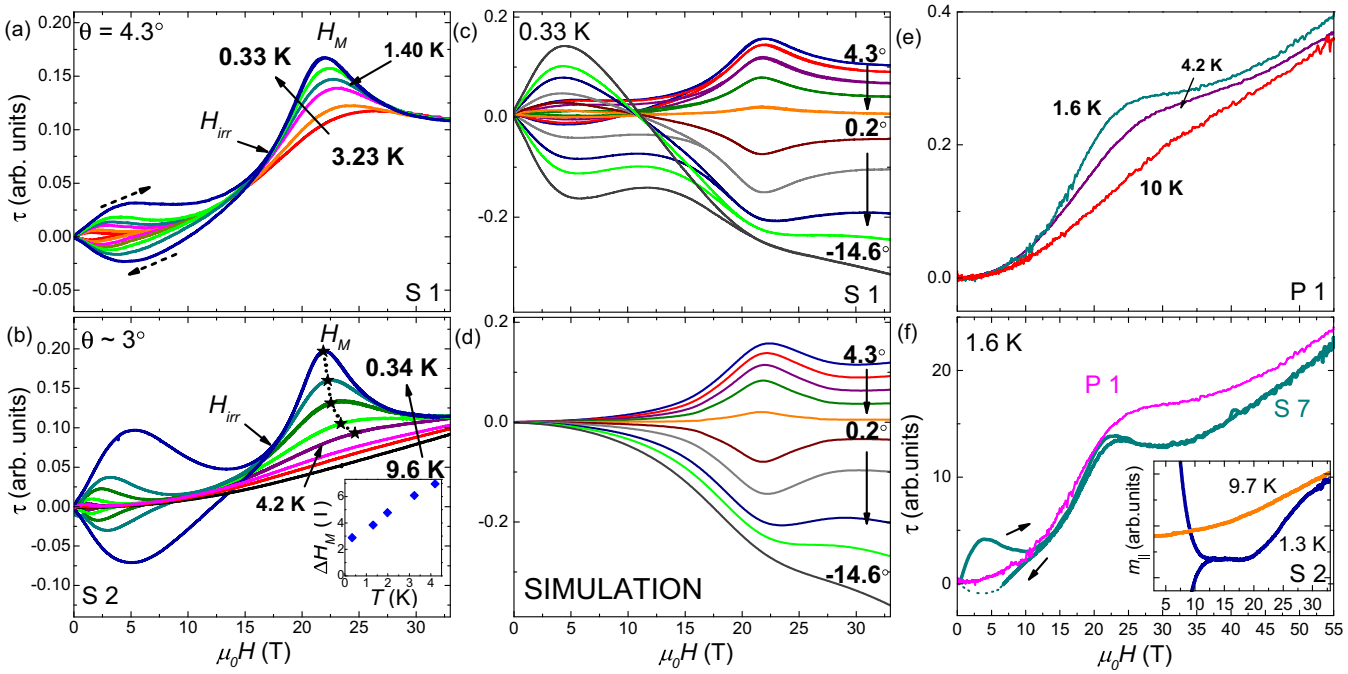

FIG. 2. (Color online) (a) Magnetic torque in an applied magnetic field at constant temperatures between 0.33 and 3.23 K for a 10-3-8 superconducting sample ($x = 0.078$) labeled S1 when $H \perp ab$ (within $\theta = 4.3^\circ$, where θ is the angle between the magnetic field and the normal to the ab planes). Solid arrows indicate the positions of the irreversibility field $\mu_0 H_{\rm irr}$ and the peak of the magnetic anomaly at $\mu_0 H_M$, dashed arrows show field sweep direction. (b) Magnetic torque vs field on sample S2 up to 9.6 K. Stars indicate the position of the maxima at $\mu_0 H_M$ determined after subtraction of the 9.6 K signal. Inset: the temperature dependence of the peak width, ΔH_M, from a Lorentzian fit. (c) Field dependence of torque as function of angle θ at 0.33 K. (d) A simulation of torque based on a spin-flop and a paramagnetic contribution described below, assuming the magnetic moments are aligned perpendicular to the ab plane in zero field. (e) Magnetic torque measurement for the parent compound ($x = 0$) labeled P1. (f) Comparison between the torque measurements for the parent ($x = 0$, sample P1) and superconducting compound ($x = 0.078$, sample S7) at 1.6 K that shows a similar behavior in a magnetic field. The inset shows the longitudinal magnetization for a superconducting sample (S2) showing a clear change in slope above the transition at $\mu_0 H_M$.

sufficiently long-lived at low temperatures to contribute to the magnetic torque. At a temperature $T \lesssim K$, where K is the single-ion magnetic anisotropy energy, the fluctuating spins at zero field lie predominantly along the easy axis and may flop under an external field; this will manifest itself in magnetic torque as a peak at H_{SF}, when the field is along the easy axis. In experiments [Figs. 2(a) and 2(b)], the sharpness of the anomaly at H_M, which we now associate with a spin-flop field H_{SF}, varies substantially between 0.33 and 3.23 K, and is completely featureless by ∼10 K. Therefore a qualitative association of the temperature and magnetic anisotropy energy scales would suggest that K is of the order of ∼1 K (86 μeV). A direct calculation of K from DFT for the Ca-10-3-8 *parent* compound ($x = 0$) gives a value of $K \approx 106$ μeV, which is of the same order of magnitude as the measured magnetic energy scale but predicts b as the easy axis. In our experimental geometry, the spin-flop explanation requires the c^* axis, perpendicular to the ab planes, to be the easy axis. This appears to be a common problem in the DFT calculatons of the magnetic ansisotropy in FeBS (see Appendix A). In principle, the spin-flop field $H_{\rm SF}$ can be estimated as $\mu_0 H_{\rm SF} = 2\sqrt{K\Delta}/M$, where M is the Fe moment and Δ is the energy difference between the ferro- and antiferromagnetic ordered states (see Appendix A). However, in the Ca-10-3-8 *parent* compound ($x = 0$) the ferromagnetic state converges only in a fixed moment calculation which results in a considerable overestimation of Δ and correspondingly, $H_{\rm SF}$ (see Appendix A).

Next, we simulate the angular dependence of torque assuming that the signal is determined by a magnetic fraction assigned to an anisotropic antiferromagnet with spins along the c^* axis with a certain Lorentzian broadening ($\Gamma \approx 2.1$ T) and choosing a spin-flop field of $H_{\rm SF} = 21.7$ T. To account for a paramagnetic fraction for the average contribution of all spins that instantaneously do not participate in the antiferromagnetic fluctuating fraction we consider an additional term $\tau \sim H^2 \times \sin 2\theta$, as described in detail in the Appendix B. While the magnetization usually shows a step or slope change at the spin-flop field, the magnetic torque as a function of applied field gives rise to a peak *only if the field is applied parallel to the easy axis* [18]. Despite the simplicity of the model, the correspondence with the experimental data above $H_{\rm irr}$ is remarkable, as shown in Fig. 2(d). Although the formula used for magnetic torque is expressed in a local moment picture, an itinerant analog of the spin flop exists [19], where the polarization vector of the spin-density wave experiences a *flop* when a sufficiently large magnetic field is applied parallel to its initially preferred direction. Thus our model assumes that the (fluctuating) magnetic moments are aligned perpendicular to the ab plane in contrast to the in-plane collinear antiferromagnetic order typically found in the parent compounds of the

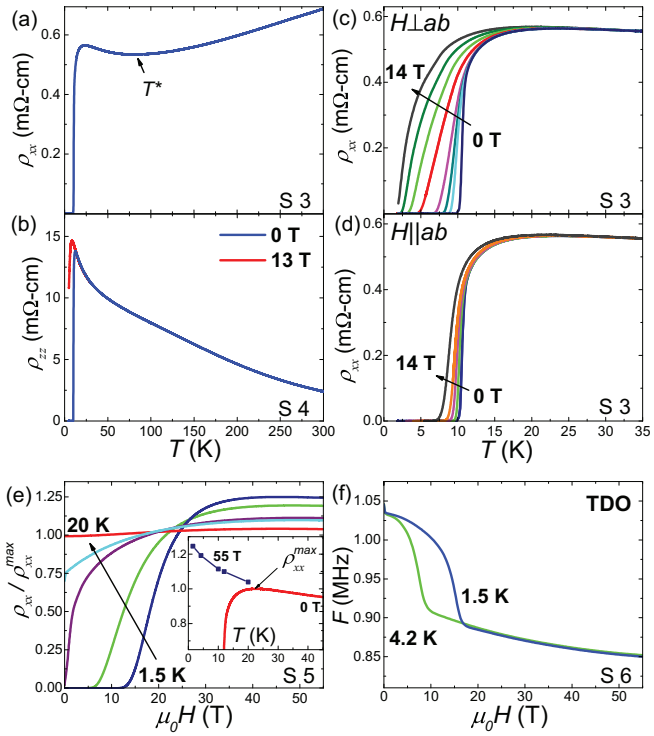

FIG. 3. (Color online) Transport measurements on single crystals of superconducting 10-3-8 ($x = 0.078$). (a) Temperature dependence of the (a) in-plane and (b) interplane resistivity in zero field. The arrow in (a) indicates the position of the minimum in resistance at T^*. Temperature dependence of in-plane resistivity in constant magnetic field (c) when $H \perp ab$ planes and (d) when $H \parallel ab$ planes. (e) Resistivity measurements in a pulsed magnetic field taken at constant temperatures. The data were normalized to the value of the sample at $\rho_{\max}$ (indicated by the arrow in inset). Inset: The normal in-plane resistivity at 55 T as a function of temperature plotted together with the zero-field resistivity. (f) TDO measurements as a function of magnetic field showing a superconducting transition but no further anomaly at 22 T.

iron-based superconductors, as calculated and expected for the parent compound of the Ca-10-3-8 ($x = 0$) compound.[3] As the anisotropy energies in these materials are not large (see Appendix A) and given the more unusual crystal structure of 10-3-8, it is sometimes possible that the easy axis is perpendicular to the ab planes. For example, neutron scattering studies suggest that in LaFeAsO, $SrFe_2As_2$, and $BaFe_2As_2$, the spins are aligned in-plane [1], but in NdFeAsO [21] along c. In the latter case, the spin flop may be masked by spin-reorientation transitions in the Nd subsystem. Additionally, polarized neutron scattering measurements in the underdoped and optimally doped $Ba(Fe_{1-x}Ni_x)_2As_2$ suggest that spin excitation anisotropy changes from c-axis polarized for optimal doping to isotropic in the overdoped regime [22,23]. In the nearly optimally doped $Ba(Fe_{0.94}Co_{0.06})_2As_2$ the low-energy spin excitations at 4 meV are also c-axis polarized [24].

[3]See Ref. [20].

III. H-T PHASE DIAGRAM

We have also performed in-plane and out-of-plane transport measurements to characterize the superconducting phase and to determine whether the transition in applied field can be detected in transport. Figure 3(a) shows the temperature dependence of the in-plane resistance that has a crossover from a metalliclike to semiconductorlike regime [8] at a temperature $T^* \approx 80$ K before it becomes superconducting at $T_c \approx 9.7$ K. A magnetic field perpendicular to the planes [Fig. 3(c)] causes a substantial broadening of the superconducting transition. However, there is a strong anisotropy and an in-plane field [Fig. 3(d)] does not suppress the transition to the same extent. This broadening indicates strong thermal fluctuations of the vortex lattice, which can be quantified by the Ginzburg number $Gi \approx 0.16$ [25], significantly higher than in typical pnictides (using a large penetration depth of $\lambda_{ab}(0) \approx 1000$ nm [25] and combined with their measured H_{c2}). In contrast to the in-plane measurements, the interplane resistance [Fig. 3(b)] increases with decreasing temperature by a factor ~6 suggesting strongly incoherent transport between the planes. In-plane resistivity [Fig. 3(e)] and penetration depth [26] [TDO in Fig. 3(f)] in very high fields up to 55 T show no anomalies that could be associated with the magnetic transition (when $H \perp ab$), beside the expected broad transition from the superconducting to the normal state. Upon suppressing the superconductivity by a magnetic field of 55 T, the normal state resistance tends to increase exponentially at low temperatures suggesting charge localization in the normal state of Ca-10-3-8, as shown in the inset of Fig. 3(e).

Based on the transport and torque data we have constructed the phase diagram of the superconducting $Ca_{10}(Pt_3As_8)((Fe_{1-x}Pt_x)_2As_2)_5$ ($x = 0.078$), as shown in Fig. 4(a). Near T_c, the anisotropy parameter $\gamma_H = H_c^{\parallel ab}(T)/H_c^{\perp ab}(T)$ is 10, characteristic of the most 2D FeBS [27,28]. For the in-plane magnetic field, we use the single-band Werthamer-Helfand-Hohenberg (WHH) model [29] and fit the zero-resistance near T_c to predict $H_{c2}(0) \approx$ 30 T, which is close to the irreversibility field of 32 T measured in torque at 1.5 K. For $H \perp ab$, the superconducting phase boundary shows a strong concave curvature that cannot be captured by the one-gap WHH model and is suggestive of multi-band superconductivity in this system, as seen in the closely related 10-4-8 superconducting phase [30] or other anisotropic systems such as the 1111 pnictides [31] and cuprates.

IV. SUMMARY

The phase diagram under pressure [12], which is similar overall to that as function of doping shown in Fig. 1 (a), tracks the minimum in the resistivity at a temperature T^* well above the structural transition, suggesting that this temperature could be linked to the gradual appearance of antiferromagnetic fluctuations (and the corresponding loss of the carrier density). Due to the more strongly two-dimensional character of Ca-10-3-8 compared to other Fe-pnictides (e.g., the long interlayer separation of 10.27 Å and the lower Néel temperature in the parent compound), antiferromagnetic spin fluctuations in the Fe-As planes without 3D long-range order are likely to exist over a large area of the phase diagram, roughly characterized

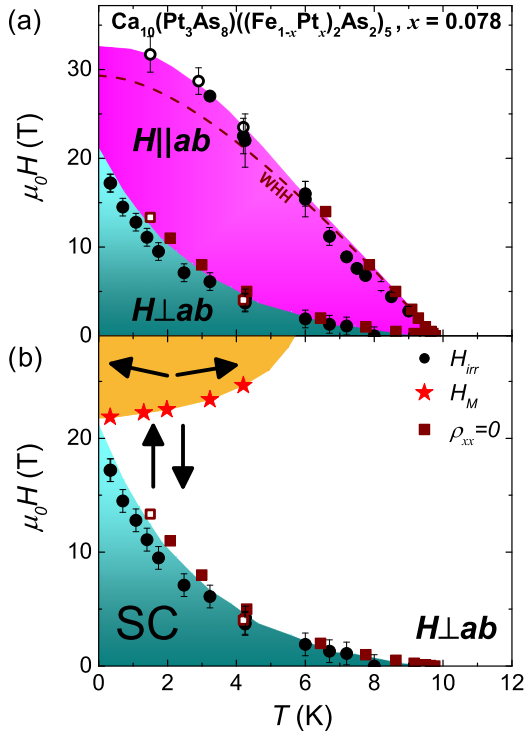

FIG. 4. (Color online) (a) The superconducting field-temperature phase diagram of nearly optimally doped $Ca_{10}(Pt_3As_8)((Fe/Pt)_2As_2)_5$ for two different orientations with respect to the (ab plane), as obtained from magnetic torque (circles) and transport measurements (squares). Open symbols indicate the pulsed fields measurements. Dashed line is the WHH fit to $H||ab$ data; the coloured phase boundaries are a guide to the eye. (b) The magnetic field-temperature phase diagram for $H \perp ab$ showing the position of the magnetic anomaly at H_M [stars - taken from Fig. 2(b)] and the irreversibility field, H_{irr} in the superconducting (SC) state. Black arrows represent the energetically favorable orientations of the fluctuating antiferromagnetic spins.

by the resistivity upturn at T^* (Fig. 1). These antiferromagnetic fluctuations may preferentially align along the c^* axis at low temperature and be responsible for the observed spin-flop-like transition in torque in an applied magnetic field both in the parent ($x = 0$) and the superconducting compound of the highly two-dimensional Ca-10-3-8 ($x = 0.078$). The signal intensity of the magnetic fraction in the superconducting compound is comparable with that of the parent phase [see comparison in Fig. 2(f)]. This implies that a similar fraction of the sample shows the same behaviour in magnetic field.

In conclusion, we have used high magnetic fields to map out the superconducting phase diagram of $Ca_{10}(Pt_3As_8)((Fe_{0.922}Pt_{0.078})_2As_2)_5$, finding a high anisotropy up to $\gamma_H = 10$, and an irreversibility field up to $\approx$32 T for $H||ab$. Most importantly, we reveal a field-induced magnetic transition at 22 T at low temperature, not previously observed in any FeBS, for both the parent and the optimally doped superconducting $Ca_{10}(Pt_3As_8)(Fe_2As_2)_5$ compounds (with $x = 0$ and 0.078, respectively). We attribute this highly unusual feature to a spin flop of antiferromagnetically fluctuating Fe moments. This thermodynamic measurement at low temperature demonstrates that the magnetic field is an effective tuning parameter of the antiferromagnetic fluctuations which may be responsible for the pairing in the 10-3-8 iron-based superconductors. Further work to quantify the nature of these magnetic fluctuations needs to be provided by other experimental techniques, such as polarized neutron scattering experiments and NMR measurements in high magnetic fields.

ACKNOWLEDGMENTS

We acknowledge fruitful discussions with Andrew Boothroyd and Andreas Kreyssig, and we thank Susie Speller for technical support. This work was supported by EPSRC (EP/I004475/1) and part of the work by the EuroMagNET II (EU Contract No. 228043). A.I.C. acknowledges an EPSRC Career Acceleration Fellowship. D.G., H.O.J., and R.V. acknowledge support from the DFG through grant SPP1458. N.N. acknowledges support from UCLA, Marie Curie fellowship (LANL) and AFOSR MURI on superconductivity. D.G. acknowledges support from the German National Academic Foundation. I.I.M. acknowledges support from the Funding Office of Naval Research (ONR) through the Naval Research Laboratory Basic Research Program, and from the Alexander von Humboldt Foundation.

APPENDIX A: A DFT APPROACH TO SPIN-FLOP TRANSITIONS

Density functional theory (DFT) calculations were done in the full-potential linear augmented plane-wave (FLAPW) framework as implemented in WIEN2K [32] with the generalized gradient approximation (GGA) by Perdew, Burke, and Ernzerhof [33] as exchange-correlation functional. We double checked our results with the FPLO [34] method where fully relativistic calculations were employed.

For calculations on the Ca-10-3-8 parent compound we considered the experimental structure as reported by Ni *et al.* [7] and constructed a $\sqrt{5} \times \sqrt{5}$ super cell in order to allow for stripe antiferromagnetism in the Fe layer. For Pt-doped Ca-10-3-8 we substituted one Fe by one Pt in the $\sqrt{5} \times \sqrt{5}$ super cell and fully relaxed the structure with a projector augmented wave basis (PAW) as implemented in VASP [35] within GGA.

The magnetic anisotropy energy was investigated by enforcing different spin orientations with inclusion of spin-orbit

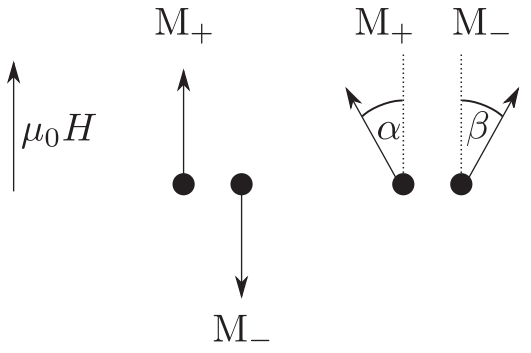

FIG. 5. Orientation of magnetic moments in the antiferromagnetic (left) and spin-flop (right) phases (for $\alpha = \beta$) used in the rigid moment model.

TABLE I. Calculated anisotropy energies and easy axes from DFT. *a* denotes the long in-plane axis perpendicular to the stripes, *b* denotes the short in-plane axis along the stripes, *c* denotes the axis perpendicular to the FeAs-planes. The lowest energy axis is set to zero. The other energy values are given relative to the lowest energy axis. Energies for $BaFe_2As_2$, $CaFe_2As_2$ and Ca-10-3-8 are given per Fe atom, while energy values for SmFeAsO are given per Sm atom. Energy values for $CaCo_2As_2$ are given per Co atom. O1 denotes the simple up-down antiferromagnetic stacking order on Co atoms, while O2 denotes the up-up-down-down order. In the Sm and Co cases the easy axis refers to Sm and Co magnetic moments, respectively.

	$BaFe_2As_2$	$CaFe_2As_2$	Ca-10-3-8	SmFeAsO	$CaCo_2As_2$ O1	O2
E_a in meV/atom	0.000	0.100	0.111	8.43	0.026	0.007
E_b in meV/atom	0.021	0.000	0.000	11.70	...	...
E_c in meV/atom	0.044	0.056	0.106	0.00	0.00	0.00
easy axis (DFT)	*a*	*b*	*b*	*c*	*c*	*c*
easy axis (exp.)	*a*	*a*	*c*	*c*	*c*	*c*

coupling in WIEN2K. In order to analyze our results, we also investigated the magnetic anisotropy in $CaFe_2As_2$, $BaFe_2As_2$ as well as $CaCo_2As_2$ (Co system) and SmFeAsO (Sm system). In the last two compounds spin-flop phases for, respectively, Co [36] and Sm [37] have been observed experimentally. For all the above systems, we considered experimental crystal structures [38–40] except for $CaCo_2As_2$. In the latter case, we used fully relaxed structures from VASP due to the absence of publications on experimental low-temperature structures. $BaFe_2As_2$ and $CaFe_2As_2$ were set up with antiferromagnetic stripe order. For SmFeAsO, we considered the experimentally observed antiferromagnetic magnetic order [41] but treated all spins collinearly, and for $CaCo_2As_2$, we considered the magnetic orders proposed in Ref. [36]. They are denoted as O1 and O2.

In order to connect the DFT calculations with the spin-flop field, we consider a system of two rigid magnetic moments without specifying the nature of exchange interactions [42]. Let Δ be the energy difference per site between the antiferromagnetic ground state and the ferromagnetic state and K be the magnetic anisotropy energy per site. Now we apply a magnetic field perpendicular to the *ab* plane. The total energy per lattice site can then be written down as the sum of the Zeeman energies of the sublattices, the exchange coupling and a term modeling the magnetic anisotropy, which makes spin-orientation perpendicular to the *ab*-plane preferable in the antiferromagnetic state [Eq. (A1)]. The orientation of the magnetic moments is measured relative to the direction of the magnetic field (see Fig. 5). The antiferromagnetic phase corresponds to $\alpha = 0$ and $\beta = \pi$ and the spin-flop phase corresponds to $\alpha = \beta$.

$$E = -\frac{\mu_0}{2} M H(\cos\,\alpha + \cos\,\beta) + \frac{\Delta}{2}\cos(\alpha+\beta) - \frac{K}{2}(\cos^2\,\alpha + \cos^2\,\beta). \quad \text{(A1)}$$

For $\alpha = \beta$, the total energy per site is given by Eq. (A2). Minimizing the energy with respect to α yields the condition $\cos\,\alpha \approx \mu_0 M H/2\Delta$, where $\Delta - K$ was approximated by Δ. Inserting this back into Eq. (A2), we obtain the expression for the energy in the spin-flop state E_{SF} [Eq. (A3)]:

$$E = -\mu_0 M H\cos\,\alpha + \frac{\Delta}{2}\cos(2\alpha) - K\cos^2\,\alpha, \quad \text{(A2)}$$

$$E_{\mathrm{SF}} = -\frac{\mu_0^2 M^2 H^2}{4\Delta} - \frac{\Delta}{2} - \frac{K\mu_0^2 M^2 H^2}{4\Delta^2}. \quad \text{(A3)}$$

The energy in the antiferromagnetic state can be obtained by inserting $\alpha = 0$ and $\beta = \pi$ into the starting equation (A1), which then reads $E_{\mathrm{AFM}} = -\frac{\Delta}{2} - K$.

The spin flop occurs when $E_{\mathrm{AFM}} > E_{\mathrm{SF}}$. This yields $\mu_0 H_{\mathrm{SF}} = 2\Delta\sqrt{K/(\Delta+K)}/M$ for the spin-flop critical field. As $K \ll \Delta$, we can safely approximate this expression by $\mu_0 H_{\mathrm{SF}} = 2\sqrt{K\Delta}/M$, which we use to estimate spin-flop fields from K, Δ and M calculated in DFT.

In Table I, we present the DFT results for the magnetic anisotropy energies. Results for the spin-flop fields $\mu_0 H_{\mathrm{SF,DFT}}$ calculated with the expression given in the main text are summarized in Table II. The anisotropy energy K was calculated

TABLE II. Calculated spin-flop fields for various parent compounds. In $BaFe_2As_2$, $CaFe_2As_2$, and Ca-10-3-8, all quantities are given per Fe atom. In SmFeAsO and $CaCo_2As_2$, all quantities are given per Sm or Co atom, respectively. O1 denotes the simple up-down antiferromagnetic stacking order on Co atoms, while O2 denotes the up-up-down-down order. In DFT, SmFeAsO and $CaCo_2As_2$ prefer ferromagnetic ordering, therefore spin-flop fields could not be estimated.

	$BaFe_2As_2$	$CaFe_2As_2$	Ca-10-3-8	SmFeAsO	$CaCo_2As_2$ O1	O2
K in meV	0.021	0.056	0.106	8.43	0.026	0.007
Δ in meV	205	179	231	−88	−2.8	−1.1
M_{DFT} in μ_B	2.0	2.0	1.9	5.2	0.64	0.66
$\mu_0 H_{\mathrm{SF,DFT}}$ in T	36	55	90	...	...	...
$\mu_0 H_{\mathrm{SF,exp}}$ in T			22	35–40	4.7	4.7

from the energy difference between the two energetically lowest antiferromagnetic states. The exchange energy Δ corresponds to the energy difference between ferromagnetic and the energetically lowest antiferromagnetic configuration. For Ca-10-3-8, a ferromagnetic solution had to be enforced by a fixed spin-moment calculation, where the single-atom magnetic moment was taken to be the same as in the DFT antiferromagnetic state. As WIEN2K does not support spin-orbit coupling in calculations with fixed spin moment, the exchange energy Δ had to be obtained without taking spin-orbit effects into account.

While the anisotropy K takes reasonable values in all investigated compounds except for SmFeAsO, the exchange Δ is strongly overestimated along with the Fe magnetic moment in $BaFe_2As_2$, $CaFe_2As_2$, and Ca-10-3-8. In $CaCo_2As_2$ and SmFeAsO, DFT predicts ferromagnetic ordering on Sm and Co, respectively, although antiferromagnetic order is observed experimentally. In $CaCo_2As_2$, this can be explained from the tiny exchange energy, which is of the right order of magnitude. For SmFeAsO, it seems that ignoring the noncollinear alignment of Sm and Fe magnetic moments leads to qualitatively wrong results.

A last point is that the preferred direction of the Fe magnetic moments in Ca-10-3-8 is predicted to be along the crystallographic b axis in DFT, which is inconsistent with our experimental observations. For $CaFe_2As_2$, DFT also finds the b axis as the easy axis, while alignment along the a axis was experimentally reported [43]. However, DFT succeeds in giving correct spin orientations for $BaFe_2As_2$, SmFeAsO, and $CaCo_2As_2$. The failure of DFT to predict the correct orientation of magnetic moments therefore seems to be a problem in the CaFeAs-based compounds.

APPENDIX B: THE SPIN-FLOP MAGNETIC TORQUE MODEL

In order to describe the observed magnetic torque, we must now consider the effect of applying a magnetic field at a general angle θ to the easy axis, rather than the special case described above. The overall shape of a magnetic torque curve is sensitive both to the overall magnetic state of a system, but also to the details of the anisotropies of the system. Here we consider the case of a material with uniaxial anisotropy (to which the layered iron-pnictide superconductors are an approximation), finding analytical forms for both paramagnetic and spin-flop contributions. Note that, due to the unusual low symmetry $P\bar{1}$ crystal structure in 10-3-8, the uniaxial anisotropy axis considered here is not the crystallographic c axis, but the c^* axis.

First, we consider a paramagnet with a uniaxially anisotropic susceptibility tensor, with no field dependence. In this case, the magnetic torque takes the form

$$\tau = \frac{\mu_0}{2}(\chi_\perp - \chi_\parallel)H^2 \sin 2\theta. \tag{B1}$$

In many layered systems an approximate H^2 dependence in torque is observed—including many Fe pnictides in their normal state beyond any superconducting hysteresis and neglecting any quantum oscillations that may appear on top of this signal. Note that this analysis depends on uniaxial symmetry and is not generally to be expected in a cubic (or other symmetry) system. Note also the general property that if there is no anisotropy (i.e., $\chi_\parallel = \chi_\perp$) then there is no torque.

In the case of an anisotropic antiferromagnet [44], the effect of a moderately large magnetic field will be dominated by the antiferromagnetic exchange energy (i.e., J), which we take to be much larger than the anisotropy energy K. Starting from an appropriate free energy F [44] and calculating $\tau = -\partial F/\partial\theta$, one can obtain [18,37]:

$$\tau = \frac{1}{2}(\chi_\perp - \chi_\parallel)\mu_0 H^2 \frac{\sin 2\theta}{\sqrt{1 - 2\lambda\cos 2\theta + \lambda^2}}, \tag{B2}$$

where we have

$$\lambda = \left(\frac{H}{H_{SF}}\right)^2 \tag{B3}$$

and

$$H_{SF} = \left[\frac{2K}{\mu_0(\chi_\perp - \chi_\parallel)}\right]^{1/2}. \tag{B4}$$

This expression [Eq. (B2)] gives a sharp peak at $H = H_{SF}$ at $\theta \to 0$, which becomes broadened as θ increases away from the symmetry axis.

In Ca-10-3-8 at $x = 0.078(6)$, we believe that the spin-flop signal arises from intermediate-ranged antiferromagnetic fluctuations located in the Fe-As planes but with an easy axis perpendicular to the plane, rather than the case of long ranged order. Therefore assigning physical values to the χ_i is not directly possible. However, if one hypothetically considers an antiferromagnetic fluctuation of many spins with time frozen then at sufficiently low temperature, it would be energetically favorable for it to align with the easy axis of the system (here, perpendicular to the Fe plane). If the magnetic field is increased, then at some point it will become favorable to spin flop into the plane, just as in the case of a long-ranged order. The magnetization, and therefore the torque, will mimic the ordered case, and there will also be a paramagneticlike contribution since the antiferromagnetism is not completely ordered. During a physical measurement, we measure an average of many such fluctuations, and it is reasonable to think that the effect of finite correlation length, fluctuation time and temperature will lead to some broadening along with crystal inhomogeneity and the unusual low-symmetry space group allowing for very slightly different Fe sites. Since magnetic torque is easily sensitive to paramagnetism, we suggest that magnetic torque would be equally sensitive to antiferromagnetic fluctuations, provided that a sufficient number of Fe sites are involved.

The angular dependence of magnetic torque in Ca-10-3-8 [$x = 0.078(6)$] is plotted in Fig. 6(a) (also in the main text), to be compared with the simulated torque in Fig. 6(b), which uses a linear combination of Eqs. (B2) and (B1). The theoretical spin-flop torque becomes arbitrarily sharp as the angle $\theta \to 0$, which is not experimentally realised. Therefore we convolute the torque with a Lorentzian broadening term with half width half maximum Γ, choosing an experimentally-motivated value for the broadening of $\Gamma = 2.1$ T, arising from the reasoning above. We set the spin-flop field H_{SF} to 21.7 T, which is the experimental peak field at $\theta \to 0$. To control the relative amplitude of the two contributions, we use the

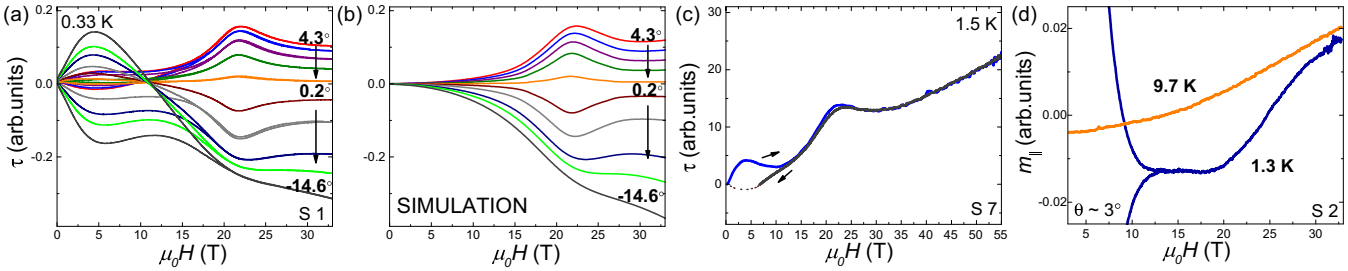

FIG. 6. (Color online) (a) Angle-dependent magnetic torque as a function of magnetic field at 0.33 K. (b) Simulation of magnetic torque incorporating a paramagnetic and spin-flop contribution, as described in the text. We have measured seven samples of 10-3-8 from the same batch in high magnetic field torque experiments, and we find quantitative agreement on the position of the spin-flop field between all samples (reproduced after Fig. 1). (c) Another sample (not shown in main text) is found to have a spin-flop transition at ∼22 T and no further anomalies are observed up to 55 T. The measurements so far have all been performed on the same batch of samples; experiments tracking the dependence of the spin flop with doping will be of much interest. (d) Using a novel technique (the gradient torque magnetometer described in the text), the component of magnetization of the sample parallel to the magnetic field is plotted. The change of slope at ∼20 T at low temperature is consistent with the spin-flop picture described.

parameter R, which is the ratio between the spin-flop and the paramagnetic torque. The paramagnetic contribution accounts for the average of all atoms that instantaneously do not participate in the antiferromagnetic spin fluctuations. When we choose a value of $R = 0.8$, the reproduction of the angle-dependence of the torque data at 0.33 K is very good for all angles, above $H_{\rm irr}$, since this model takes no account of the hysteretic torque arising from the pinning of superconducting vortices.

APPENDIX C: MAGNETIZATION IN MAGNETIC FIELDS

In order to better characterise the nature of the transition observed in magnetic torque experiments, we used a field-gradient torque magnetometer. The novel technique, developed particularly for small samples in high magnetic fields [45], involves subtracting signals of torque measurements with and without a large field gradient applied by a small neodymium piece close to (or far from) the sample, the difference being attributable to a term proportional to $\mathbf{m} \cdot \nabla \mathbf{B}$, i.e., the magnetization component $m_\parallel$ parallel to the magnetic field. The raw torque (i.e., without the field gradient) is $\mathbf{m} \times \mathbf{B}$, i.e., sensitive to $m_\perp$—the component of magnetization perpendicular to the applied field. Therefore the method allows simultaneous measurements of both components of the magnetization. The raw torque is plotted in Fig. 1(b) in the main text, and the magnetization is plotted in Fig. 6(d) showing a large hysteretic superconducting signal at low temperature below $H_{\rm irr}$. At ∼20 T there is a clear kink marking the spin-flop transition. The onset field departs slightly from the spin-flop field of 21.7 T due to the finite angle and broadening. The form of the transition can be easily understood since in the antiferromagnetic state there is no net magnetization, whereas in the spin-flop state, there is an increasing magnetization along the direction of the field as the Zeeman energy makes this increasingly favorable.

[1] M. D. Lumsden and A. D. Christianson, J. Phys.: Condens. Matter **22**, 203203 (2010).

[2] S. Kasahara, H. J. Shi, K. Hashimoto, S. Tonegawa, Y. Mizukami, T. Shibauchi, K. Sugimoto, T. Fukuda, T. Terashima, A. H. Nevidomskyy, and Y. Matsuda, Nature (London) **486**, 382 (2012).

[3] T. Shimojima, T. Sonobe, and W. Malaeb, Phys. Rev. B **89**, 045101 (2014).

[4] J.-H. Chu, H.-H. Kuo, J. G. Analytis, and I. R. Fisher, Science **337**, 710 (2012).

[5] R. M. Fernandes, L. H. VanBebber, S. Bhattacharya, P. Chandra, V. Keppens, D. Mandrus, M. A. McGuire, B. C. Sales, A. S. Sefat, and J. Schmalian, Phys. Rev. Lett. **105**, 157003 (2010).

[6] R. M. Fernandes, A. V. Chubukov, J. Knolle, I. Eremin, and J. Schmalian, Phys. Rev. B **85**, 024534 (2012).

[7] N. Ni, J. M. Allred, B. C. Chan, and R. J. Cava, Proc. Natl. Acad. Sci. USA **108**, E1019 (2011).

[8] Z. J. Xiang, X. G. Luo, J. J. Ying, X. F. Wang, Y. J. Yan, A. F. Wang, P. Cheng, G. J. Ye, and X. H. Chen, Phys. Rev. B **85**, 224527 (2012).

[9] K. Cho, M. A. Tanatar, H. Kim, W. E. Straszheim, N. Ni, R. J. Cava, and R. Prozorov, Phys. Rev. B **85**, 020504 (2012).

[10] T. Zhou, G. Koutroulakis, J. Lodico, N. Ni, J. D. Thompson, R. J. Cava, and S. E. Brown, J. Phys.: Condens. Matter **25**, 122201 (2013).

[11] T. Stürzer, G. M. Friederichs, H. Luetkens, A. Amato, H.-H. Klauss, and D. Johrendt, J. Phys.: Condens. Matter **25**, 122203 (2013).

[12] P. Gao, L. Sun, N. Ni, J. Guo, Q. Wu, C. Zhang, D. Gu, K. Yang, A. Li, S. Jiang, R. J. Cava, and Z. Zhao, Adv. Mater. **26**, 2346 (2014).

[13] N. Ni, W. E. Straszheim, D. J. Williams, M. A. Tanatar, R. Prozorov, E. D. Bauer, F. Ronning, J. D. Thompson, and R. J. Cava, Phys. Rev. B **87**, 060507 (2013).

[14] M. Neupane, C. Liu, S.-Y. Xu, Y.-J. Wang, N. Ni, J. M. Allred, L. A. Wray, N. Alidoust, H. Lin, R. S. Markiewicz, A. Bansil, R. J. Cava, and M. Z. Hasan, Phys. Rev. B **85**, 094510 (2012).

[15] S. Thirupathaiah, T. Stürzer, V. B. Zabolotnyy, D. Johrendt, B. Büchner, and S. V. Borisenko, Phys. Rev. B **88**, 140505 (2013).

[16] A. I. Coldea, J. D. Fletcher, A. Carrington, J. G. Analytis, A. F. Bangura, J.-H. Chu, A. S. Erickson, I. R. Fisher, N. E. Hussey, and R. D. McDonald, Phys. Rev. Lett. **101**, 216402 (2008).
[17] C. Putzke, A. I. Coldea, I. Guillamón, D. Vignolles, A. McCollam, D. LeBoeuf, M. D. Watson, I. I. Mazin, S. Kasahara, T. Terashima, T. Shibauchi, Y. Matsuda, and A. Carrington, Phys. Rev. Lett. **108**, 047002 (2012).
[18] T. Kawamoto, Y. Bando, T. Mori, T. Konoike, Y. Takahide, T. Terashima, S. Uji, K. Takimiya, and T. Otsubo, Phys. Rev. B **77**, 224506 (2008).
[19] G. Varelogiannis, Phys. Rev. Lett. **91**, 117201 (2003).
[20] Andreas Kreyssig (private communication).
[21] A. Marcinkova, T. C. Hansen, and J. W. G. Bos, J. Phys.: Condens. Matter **24**, 256007 (2012).
[22] M. Liu, C. Lester, J. Kulda, X. Lu, H. Luo, M. Wang, S. M. Hayden, and P. Dai, Phys. Rev. B **85**, 214516 (2012).
[23] H. Luo, M. Wang, C. Zhang, X. Lu, L.-P. Regnault, R. Zhang, S. Li, J. Hu, and P. Dai, Phys. Rev. Lett. **111**, 107006 (2013).
[24] P. Steffens, C. H. Lee, N. Qureshi, K. Kihou, A. Iyo, H. Eisaki, and M. Braden, Phys. Rev. Lett. **110**, 137001 (2013).
[25] J. Kim, F. Ronning, N. Haberkorn, L. Civale, E. Nazaretski, N. Ni, R. J. Cava, J. D. Thompson, and R. Movshovich, Phys. Rev. B **85**, 180504 (2012).
[26] L. Drigo, F. Durantel, A. Audouard, and G. Ballon, Eur. Phys. J. Appl. Phys. **52**, 10401 (2010).
[27] A. Carrington, A. Coldea, J. Fletcher, N. Hussey, C. Andrew, A. Bangura, J. Analytis, J.-H. Chu, A. Erickson, I. Fisher, and R. McDonald, Physica C **469**, 459 (2009).
[28] H. Q. Yuan, J. Singleton, F. F. Balakirev, S. A. Baily, G. F. Chen, J. L. Luo, and N. L. Wang, Nature (London) **457**, 565 (2009).
[29] N. R. Werthamer, E. Helfand, and P. C. Hohenberg, Phys. Rev. **147**, 295 (1966).
[30] E. Mun, N. Ni, J. M. Allred, R. J. Cava, O. Ayala, R. D. McDonald, N. Harrison, and V. S. Zapf, Phys. Rev. B **85**, 100502 (2012).
[31] J. Jaroszynski, F. Hunte, L. Balicas, Y.-J. Jo, I. Raičević, A. Gurevich, D. C. Larbalestier, F. F. Balakirev, L. Fang, P. Cheng, Y. Jia, and H. H. Wen, Phys. Rev. B **78**, 174523 (2008).
[32] P. Blaha, K. Schwarz, G. K. H. Madsen, D. Kvasnicka, and J. Luitz, WIEN2K, *An Augmented Plane Wave + Local Orbitals Program for Calculating Crystal Properties* (Technische Universitt Wien, Wien, Austria, 2001).
[33] J. P. Perdew, K. Burke, and M. Ernzerhof, Phys. Rev. Lett. **77**, 3865 (1996).
[34] K. Koepernik and H. Eschrig, Phys. Rev. B **59**, 1743 (1999).
[35] G. Kresse and J. Furthmüller, Phys. Rev. B **54**, 11169 (1996).
[36] B. Cheng, B. F. Hu, R. H. Yuan, T. Dong, A. F. Fang, Z. G. Chen, G. Xu, Y. G. Shi, P. Zheng, J. L. Luo, and N. L. Wang, Phys. Rev. B **85**, 144426 (2012).
[37] S. Weyeneth, P. J. W. Moll, R. Puzniak, K. Ninios, F. F. Balakirev, R. D. McDonald, H. B. Chan, N. D. Zhigadlo, S. Katrych, Z. Bukowski, J. Karpinski, H. Keller, B. Batlogg, and L. Balicas, Phys. Rev. B **83**, 134503 (2011).
[38] M. Rotter, M. Tegel, D. Johrendt, I. Schellenberg, W. Hermes, and R. Pottgen, Phys. Rev. B **78**, 020503 (2008).
[39] A. Kreyssig, M. A. Green, Y. Lee, G. D. Samolyuk, P. Zajdel, J. W. Lynn, S. L. Bud'ko, M. S. Torikachvili, N. Ni, S. Nandi, J. B. Leão, S. J. Poulton, D. N. Argyriou, B. N. Harmon, R. J. McQueeney, P. C. Canfield, and A. I. Goldman, Phys. Rev. B **78**, 184517 (2008).
[40] S. Margadonna, Y. Takabayashi, M. T. McDonald, M. Brunelli, G. Wu, R. H. Liu, X. H. Chen, and K. Prassides, Phys. Rev. B **79**, 014503 (2009).
[41] S. Nandi, Y. Su, Y. Xiao, S. Price, X. F. Wang, X. H. Chen, J. Herrero-Martin, C. Mazzoli, H. C. Walker, L. Paolasini, S. Francoual, D. K. Shukla, J. Strempfer, T. Chatterji, C. M. N. Kumar, R. Mittal, H. M. Ronnow, C. Rüegg, D. F. McMorrow, and T. Brückel, Phys. Rev. B **84**, 054419 (2011).
[42] S. Blundell, *Magnetism in Condensed Matter* (Oxford University Press, Oxford, 2010).
[43] A. I. Goldman, D. N. Argyriou, B. Ouladdiaf, T. Chatterji, A. Kreyssig, S. Nandi, N. Ni, S. L. Bud'ko, P. C. Canfield, and R. J. McQueeney, Phys. Rev. B **78**, 100506 (2008).
[44] K. Yosida, Prog. Theor. Phys. **6**, 356 (1951).
[45] A. McCollam, P. G. van Rhee, J. Rook, E. Kampert, U. Zeitler, and J. C. Maan, Rev. Sci. Instrum. **82**, 053909 (2011).